Modeling Tool for Capacitive RF MEMS Operating Bias Voltage Optimization

Anne-Charlotte Amiaud, Aude Leuliet, Brigitte Loiseaux, Julien Nagle, Paolo Martins, Raphael Aubry, Stephane Hole

Modeling tool for capacitive RF MEMS operating bias voltage optimization

Anne-Charlotte Amiaud[a], Aude Leuliet[a,*], Brigitte Loiseaux[a], Julien Nagle[a], Paolo Martins[a], Raphaël Aubry[a] and Stéphane Holé[b]

[a] *Thales Research and Technology, F-91767 Palaiseau, France*

[b] *LPEM, Université Pierre et Marie Curie – Paris6, France*

***Abstract*—In this paper, dielectric charging process in dielectrics under bias voltage is investigated. Dielectric materials, used in numerous devices in microelectronics, can be subjected to significant electrical stress. These high electric fields impact the device lifetime. Actuation voltage measurements of capacitive RF MEMS as a function of stress time have been performed. Results show that the actuation voltage varies because of charge storage in the dielectric thin film. In this work a simulation code has been developed to model charge transport phenomena in insulators. This model takes into account tunnel and thermal effects in the dielectric and at the dielectric-metal interfaces. Thanks to this model, charge carrier distribution in the dielectric layer can be calculated. The actuation bias shift versus time, which can be responsible for RF capacitive structure failure, can also be determined. Experimental results can be reproduced thanks to simulations. This simulation tool is then used to define the optimal operating voltage value for a given RF MEMS device. It may also be used to assist in device design in microelectronics. Indeed for a given material set, the optimal operating voltage value is calculated as a function of device properties.**

***Index Terms*—microelectronics, reliability, modeling, dielectric materials, electrical stress, charge accumulation**

I. Introduction

CAPACITIVE Radio-frequency microelectromechanical system (RF MEMS) switches are micro scale components used as actuators. Shunt RF MEMS switches consist of a bottom electrode, a thin dielectric layer (thickness of about 100 nm) and a movable top electrode integrated on a coplanar line. The top electrode or membrane is pulled down into contact with the dielectric layer by applying the required bias voltage (pull-in voltage V_{pi}); the capacitance increases and the radio-frequency signal is cut off. When the bias is zero, the top electrode moves up, the isolation decreases and the signal can pass. These devices present some advantages: low-power consumption, low insertion loss and very compact size. However there are well known reliability issues: contact degradation between dielectric and movable top electrode, mechanical fatigue [1] and dielectric charging effects, which limit the device lifetime [2] [3] [4]. In this paper we are particularly focused on dielectric charging. When the actuation bias is applied, the top electrode is pulled-down and some charges can be injected from the metal electrode into dielectric traps [5] [6]. These charges cannot be evacuated when operating the switch and thus remain stored in the dielectric layer. This modifies electrostatic forces applied on the top electrode. It leads to a drift of the actuation voltage [7] and to the failure of the structure by blocking the top electrode in up or down state [4] [8] [9]. A key issue to solve such a reliability problem and optimize the device lifetime is the understanding of charge accumulation mechanisms and the tuning of dielectric electrical properties [10]. Numerous models have been developed to estimate the dielectric charging effect on component performances depending on material, component design and operating conditions [11] [12] [13] [14] [15]. Most of them are not designed to study the charge transport mechanisms in the insulator and the time evolution of physical quantities in the whole dielectric layer. However, to control charge accumulation and then improve component reliability it is necessary to understand dielectric charging process.

Our study is focused on devices fabricated with silicon nitride dielectric layers deposited by Plasma Enhanced Chemical Vapor Deposition at 340°C. First, RF MEMS switches are characterized according to dielectric charging study. Then, a one dimensional dielectric charging model based on solving both Poisson and charge continuity equations is presented. Electric field, current and charge carrier distribution are calculated in the whole dielectric layer as a function of time. We will show how this model allows computing the amount of charges and their location in the dielectric. Simulation and experimental measurement results are in good agreement. This simulation tool is able to optimize capacitive RF MEMS operating conditions and to assist in microelectronic device design.

II. Measurements

A. Samples

Measurements are performed on capacitive RF MEMS shunt switches with silicon nitride as insulator (Figure 1). The dielectric thin layer integrated in these capacitive structures has a thickness of 255 nm and is deposited by Plasma Enhanced Chemical Vapor Deposition (PECVD) at 340°C. The bottom electrode consists of a gold layer and a thin Ti layer (10 nm), the dielectric film is deposited on this static electrode. The top electrode consists of a bilayer TiW/Au (Figure 2).

* Corresponding author :E-mail address : aude.leuliet@thalesgroup.com

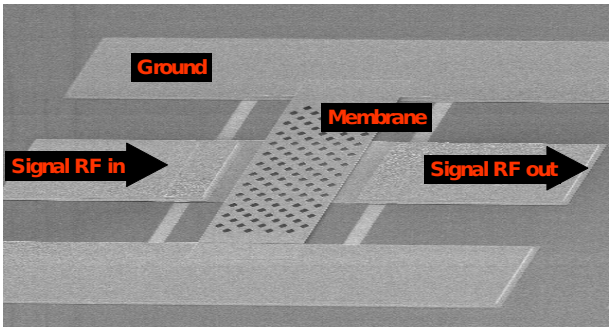

Figure 1 : SEM picture of a shunt RF MEMS.

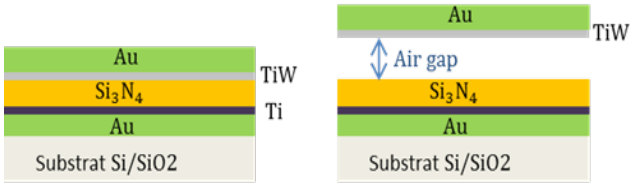

Figure 2 : Schematic cross section of the capacitive RF MEMS central part at low state (left) and up state (right). In down state, the silicon nitride layer is sandwiched between the Au/Ti bottom electrode and the TiW/Au membrane.

B. Device characterization

Capacitive RF MEMS have been characterized. The pull-in voltage temporal evolution has been measured in two steps: the cycling (aging test) and the pull-in voltage evaluation. During the cycling part, voltage pulses are applied on the device. The top electrode goes down when the applied bias increases and goes up when the applied bias decreases to zero. At the same time, S parameters at 10 GHz are measured with a vector network analyzer to evaluate losses (S_{11} parameter) and isolation (S_{21} parameter) versus the applied electric stress. When the top electrode moves down, the isolation increases; when the top electrode moves up, the isolation decreases. The pull-in voltage is then regularly measured thanks to triangular voltage ramps. This is the applied voltage value for which the isolation sharply increases. The initial pull-in voltage $V_{pi}(t_0)$ of the device is estimated to $49\,V$. The component is subjected to millions of $60\,V$ pulses during the experiment.

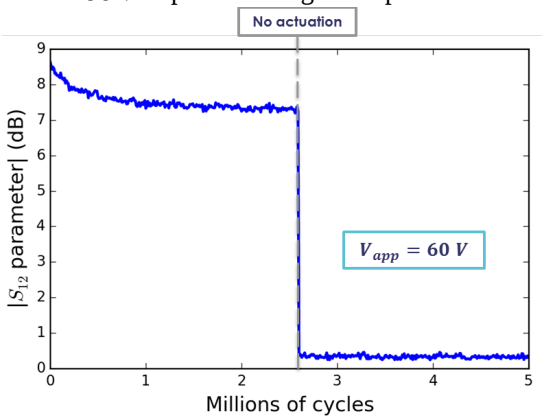

Figure 3 : Absolute value of the MEMS isolation measured at 10GHz as a function of the number of cycles (in millions).

The isolation as a function of the number of cycles is measured at $60\,V$ for each voltage pulse performed during the experimental test (Figure 3). The isolation decreases at the beginning of the measurement, the contact area between the dielectric and the top electrode decreases. After 2,5 millions of cycles, the isolation decreases sharply, the top electrode can no longer move down at $60\,V$. The applied voltage is not enough to enable switching. The triangular voltage ramp allows obtaining the pull-in voltage temporal evolution (Figure 4). It increases with the number of cycles until the device actuation is stopped.

In the literature, several reasons are proposed to explain this pull-in voltage evolution during the device operating time. It may be due for example to modification of the mechanical properties of the top electrode or to charge storage in the dielectric thin film [1] [16] [17].

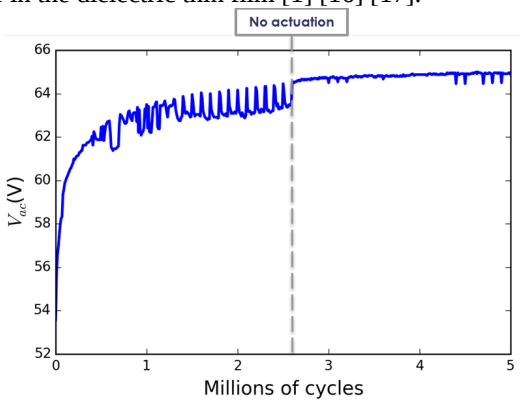

Figure 4 : Pull-in bias as a function of number of cycles for $V_{app}=60\,V$ actuation bias measured thanks to the triangular ramp is shifted compared to measurements performed with square pulses of different bias voltage. Indeed when V_{acc} is applied to the structure, the membrane moves down and the maximum isolation is obtained after the membrane actuation time. At this moment the voltage applied to the structure is higher due to the ramp shape of the stress. Here V_{acc} is shifted of around +5 V.

The tested device is then rested for a day and a new set of cycles is carried out, but the component is still not working at $60\,V$. By performing the first experiment with an applied bias of $-60\,V$, the device is operational once again. This experimental result shows that the device non actuation at 60V probably stems from charge storage in the dielectric.

By plotting the isolation as a function of the applied bias for the first voltage ramp, that is the initial state, and for the voltage ramp after 5 millions of cycles, we can observe that the curve is shifted without distortion (Figure 5). This shift is related to dielectric charging [8] [18] [19]. Moreover, the curve is only shifted and not distorted; this states that the charge is evenly distributed in the plane of the dielectric thin layer [2] [4]. The curve is shifted to the higher voltage values, charge stored in the dielectric is negative [4] [20]. The bias is applied on the bottom electrode; charges are injected from the top electrode into the dielectric film.

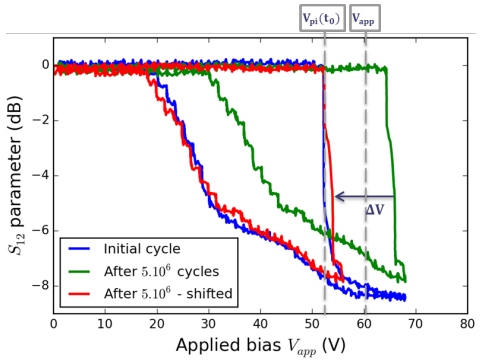

Figure 5 : Isolation as a function of applied bias for a capacitive RF MEMS at initial state (blue) and after 5 millions of cycles (green). The red curve represents the isolation after 5 millions of cycles shifted of 12 V. It is superimposed on the initial curve showing that there is no curve distortion.

III. MEMS RELIABILITY MODELING

A. *Charge transport model*

A dielectric charging model under electrical stress has been developed for Metal-Insulator-Metal (MIM) capacitors, simple devices. It is a one-dimensional model; calculation is performed in the dielectric thickness. It can be used for simulations involving charge and discharge steps. This general model is realized for capacitive structures with silicon nitride as insulator layer currently used in microelectronics. However, this model can be used to study other insulator materials under electric field.

Different charge transport mechanisms are considered in the model (Figure 6). The Schottky effect is proposed in the literature as injection mechanism [9]. It enables charges injection into the dielectric conduction band by thermal effect. The Trap Assisted Tunneling (TAT) current is also responsible of charge injection in silicon nitride [21] [22]. Charges are injected into dielectric traps by tunnel effect or are extracted from dielectric traps into electrode by tunnel effect (TATre) [23]. Trapping and detrapping mechanisms (including Frenkel-Poole effect [9] [21] [24]) and Space Charge Limited Current [9] are considered for bulk transport mechanisms (Figure 6).

The one dimensional model for charge transport in dielectric films under bias voltage is based on the numerical resolution of the following equations:

$$\frac{\partial E(z,t)}{\partial z} = \frac{\rho(z,t)}{\varepsilon_0 \varepsilon_r} \quad \text{(Poisson equation) (1)}$$

$$\frac{\partial \rho(z,t)}{\partial t} = \frac{-\partial j(E,z,t)}{\partial z} \quad \text{(Charge conservation relation) (2)}$$

where ρ is the bulk density of carriers, j the current density and E is the electric field. The dielectric is discretized in slices of index i and thickness dz and a bias voltage (V_{app}) is applied between the first and the last slice with the boundary condition: $\sum_i E_i d z_i = -V_{app}$.

These equations are solved for each layer and each time step. The time and spatial dependence of the different physical quantities is determined by the resolution of time and spatial dependent physical equations.

The following assumptions have been made for the modeling: i) homogeneous dielectric layer, ii) traps uniformly distributed in the dielectric, iii) only one type of trap, iv) dielectric film without charges at the beginning of the calculation and v) roughness of the metal-dielectric interfaces neglected.

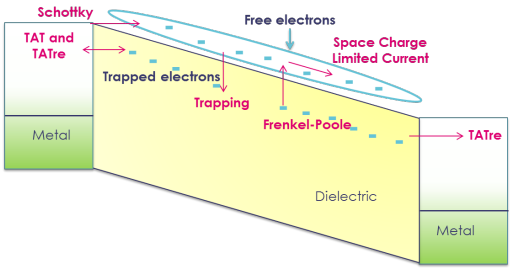

Figure 6. Dielectric charging model.

B. *Simulation-Measurement comparisons*

This model gives an access to the spatial charge distribution in the whole dielectric thin layer as a function of time (Figure 7). So the impact of this charge accumulation on the pull-in voltage can be estimated during the simulation. The calculation of the pull-in voltage shift ΔV is the sum of each contribution of the different insulator slices i CITATION XYu06 \l 1036 [25] :

$$\Delta V = \frac{1}{\varepsilon_0 \varepsilon_r} \sum_{j=0}^{N} \sum_{i=0}^{j} \rho_i dx_i dx_j \qquad (3)$$

with ε_r the relative permittivity of the dielectric, d_i the distance between the bottom electrode and the slice i with surface charge density ρ_i . It is a one dimensional model, so the charge is assumed to be laterally uniformly distributed in the dielectric ~~plan~~. Simulation results can be compared to pull-in voltage measurements; experimental results show that the injected charge in the dielectric is actually laterally evenly distributed.

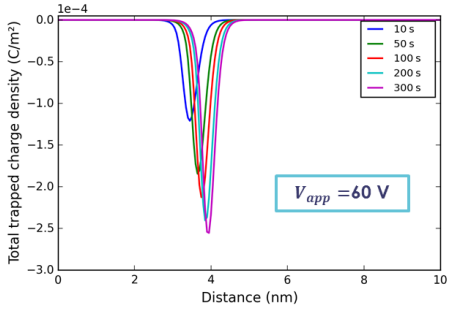

Figure 7 : Trapped charge spatial distribution in the dielectric thin film after different electrical stress times

As the RF MEMS is at low state, charges can be injected in the dielectric by the top electrode. As the stress is cut off, the top electrode moves up and no charge can be injected but they can move within the insulator layer. Figure 4 shows that the pull-in voltage does not decrease after the device non actuation at 60V. The dielectric does not seem to discharge,

carriers cannot reach the bottom electrode. Moreover, as previously exposed, the component is still not working at $60\,V$ after a rest of 24 hours. The discharge is slow compared to charge process and is neglected for RF MEMS cycling simulation. Only the cumulative actuated time is considered [6].

Simulations have been performed in order to study the pull-in voltage as a function of the stress time. Our model allows reproducing the measurement results for several applied voltages (Figure 8). The parameter values used for these simulations are given Table I.

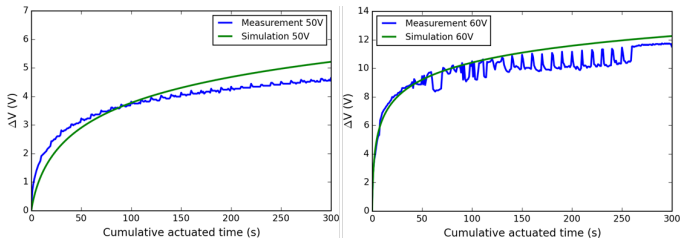

Figure 8 : Pull-in shift simulation-measurement comparisons as a function of the cumulative actuated time.

The contact between the top electrode, the injection electrode in the studied case, and the dielectric layer is different for a capacitor and for a capacitive RF MEMS. Indeed, for the RF MEMS the top electrode is in contact with the dielectric film during the actuation but this is a weak contact as there is no bonding chemical reactions at this interface as it is the case in MIM capacitor. Moreover, due to the roughness, contacts between materials are point contacts and there are small air gaps. The interface is then different; charge injection mechanisms are not the same. For the point contacts, charges can be injected in the dielectric by tunnel or thermal effects, equivalent to Schottky or TAT mechanisms. For the air gaps, charges transport mechanisms are different. A partial discharge may occur in the air; ionized particles drift under the influence of the electric field. These charges can be injected into the insulator. Effects linked to the measurement environmental conditions (for example humidity [26]) and the presence of the air gap can impact the interface area properties.

Finally, the proposed model allows reproducing the pull in voltage dependence as a function of the stress time without taking into account some particular physical phenomena at the interfaces. They could be considered in the model by the introduction of an effective medium including dielectric and air at the interface between the dielectric and the top movable electrode.

C. *Device lifetime optimization*

Simulation-measurement comparisons allow obtaining the material parameter values of the capacitive device studied. From these results, it is possible to perform complementary simulations in order to evaluate the total amount of charges in the dielectric and the induced pull-in voltage shift depending on the applied bias (Figure 9). In our case, the pull-in voltage shift can vary from few volts for an electrical stress of 50 V for 300 s to about 25 V for an electrical stress of 75 V for 300 s. The higher the applied bias, the higher the pull-in voltage shift.

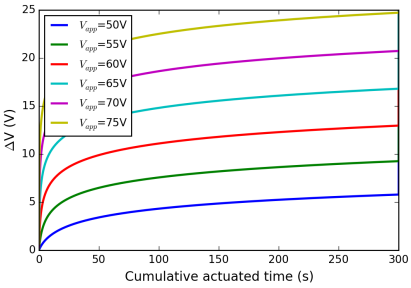

Figure 9 : Pull-in bias shift as a function the cumulative actuated time for different applied voltage values

If the same material set is used to design another RF MEMS with a given pull-in voltage at the initial state $V_{pi}(t_0)$, the simulation code can help to find the optimal applied bias value to improve the component lifetime. For example, if $V_{pi}(t_0)=50\,V$ and if $V_{app}=55\,V$, the device will no longer operate after $\tau_{¿}=¿$ 19 s under electrical stress.

TABLE I
PHYSICAL PARAMETER VALUES FOR THE SIMULATION

Parameter	Value
TAT barrier	$1{,}48\,eV$
Schottky barrier	$1{,}3\,eV$
Trap density (for $dz=0{,}5\,Å¿$	$1\times10^{16}/m^2$
Trap energy	$0{,}77\,eV$
Bulk relative permittivity	6,3
Interfacial relative permittivity	7,5
Effective mass	$0{,}6\,m_0$

The top electrode cannot be actuated if the following criterion is not fulfilled:

$$V_{pi}(t_0)+\Delta V \le V_{app} \qquad (4)$$

For this particular example, we observe that if the applied bias on the device increases against the initial pull-in voltage, this criterion is longer fulfilled (Figure 10).

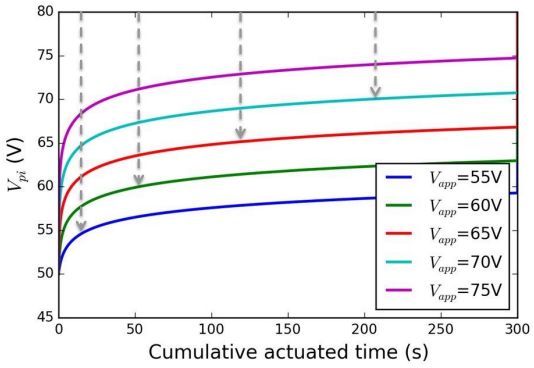

Figure 10 : Pull-in bias shift as a function the

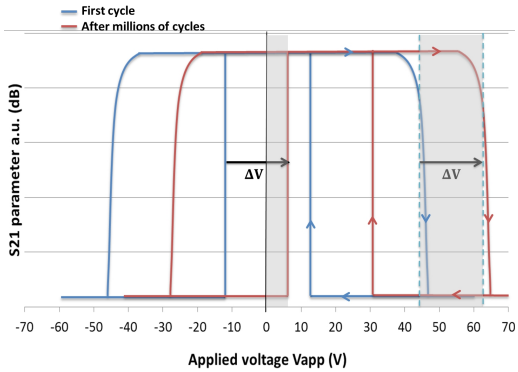

Figure 11: Schematic diagram of the isolation as a function of the applied voltage at initial state and after millions of cycles

An applied bias much higher than the initial pull-in voltage seems to improve the device lifetime. However, two other physical quantities have to be taken into account to enhance capacitive RF MEMS performances: the dielectric voltage breakdown and the top electrode holding voltage V_h . If ΔV is above the holding voltage, the top electrode stays at low state it the applied voltage is zero [18] (Figure 11). If the following criterion is not fulfilled there is a stiction of the top electrode:

$$-V_h + \Delta V \leq 0 \qquad (5)$$

It is necessary to optimize the device operating voltage depending on these two criteria.

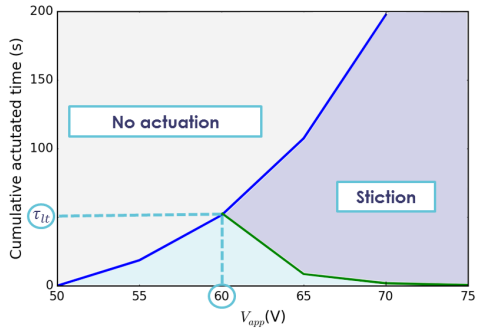

Figure 12 : Capacitive RF MEMS behavior as a function of the applied voltage - Optimal operating voltage evaluation for a device having an initial pull-in at 50V.

Knowing $V_{pi}(t_0)$ and V_h (imposed by the device design), an optimal operating voltage V_{opt} can be determined thanks to simulations. Simulation results allow plotting a graph showing the (4) and the (5) criteria as a function of the applied bias on the device (Figure 12). For example if $V_{pi}(t_0)=50V$ and $V_h=10V$, the optimal operating voltage of the device given by the simulation is $V_{opt}=60V$. For a given device structure and a given material set, the calculation code allows finding the voltage value to be applied to improve the component lifetime. Indeed, if the same material set is used for several designs and so different pull-in and holding voltages, we can calculate the optimal operating voltage thanks to simulation results. So it becomes possible to optimize the component design and improve capacitive RF MEMS lifetime for a given material set (Table II and Table III). These results help to define device structures depending on material used.

TABLE II
TIME TO DEVICE ACTUATION STOP FOR 300 S STRESS AS A FUNCTION OF THE PULL-IN VOLTAGE

V_{app}	$V_{pi}(t_0)=40$	$V_{pi}(t_0)=50$	$V_{pi}(t_0)=60$
45 V	$\tau_{¿}>300\,s$	×	×
50 V	$\tau_{¿}>300\,s$	×	×
55 V	$\tau_{¿}>300\,s$	$\tau_{¿}=18{,}6\,s$	×
60 V	$\tau_{¿}>300\,s$	$\tau_{¿}=51{,}4\,s$	×
65 V	$\tau_{¿}>300\,s$	$\tau_{¿}=107{,}5\,s$	$\tau_{¿}=0{,}7\,s$
70 V	$\tau_{¿}>300\,s$	$\tau_{¿}=197{,}5\,s$	$\tau_{¿}=1{,}8\,s$
75 V	$\tau_{¿}>300\,s$	$\tau_{¿}>300\,s$	$\tau_{¿}=3{,}5\,s$

IV. Conclusion

In this paper, the dielectric charging process in capacitive RF MEMS switches is investigated. The drift of the pull-in voltage measured on capacitive RF MEMS, with silicon nitride as insulator, is due to the insulator charging process. To study this phenomenon, a physical model based on several conduction mechanisms at the interfaces and in the dielectric bulk has been developed. With this model, the charge spatial distribution is calculated in the dielectric thanks to both Poisson and charge continuity equations. So it becomes possible to calculate the pull-in voltage drift and compare with measurement results. There is a good agreement between measurement and simulation results; this model can be used to evaluate device lifetime. Simulations have been performed for different applied bias in order to calculate the pull-in voltage drift as a function of operating conditions. These results allow finding the optimal applied voltage value to improve device lifetime. This calculation code can be used to optimize the lifetime of existing devices and help for the design of new devices to improve their reliability.

TABLE III
Time to device actuation stop for 300 s stress as a function of the holding voltage

V_{app}	$V_h = 10\,V$	$V_h = 15\,V$	$V_h = 20\,V$
45 V	$\tau_{¿} > 300\,s$	$\tau_{¿} > 300\,s$	$\tau_{¿} > 300\,s$
50 V	$\tau_{¿} > 300\,s$	$\tau_{¿} > 300\,s$	$\tau_{¿} > 300\,s$
55 V	$\tau_{¿} > 300\,s$	$\tau_{¿} > 300\,s$	$\tau_{¿} > 300\,s$
60 V	$\tau_{¿} = 53\,s$	$\tau_{¿} > 300\,s$	$\tau_{¿} > 300\,s$
65 V	$\tau_{¿} = 8{,}4\,s$	$\tau_{¿} = 110{,}4\,s$	$\tau_{¿} > 300\,s$
70 V	$\tau_{¿} = 1{,}8\,s$	$\tau_{¿} = 17{,}1\,s$	$\tau_{¿} = 202{,}7\,s$
75 V	$\tau_{¿} = 0{,}5\,s$	$\tau_{¿} = 3{,}6\,s$	$\tau_{¿} = 30{,}7\,s$

References

[1] X. Yan, W. Brown, Y. Li, J. Papapolymerou, C. Palego, J. Hwang et R. Vinci, «Anelastic stress relaxation in gold films and its impact on restoring forces in MEMS switch application," *Microelectronics engineering*, vol. 162, p. 89, 2016.

[6] S.Mellé, D.DeConto, D.Dubuc, K.Grenier, O.Vendier, J-L.Muraro, J-L.Cazaux and R.Plana, "Reliability modeling of capacitive RF MEMS," *IEEE Transactions on Microwave Theory and techniques*, vol. 53, November 2005.

[7] A.Koszewski, F.Souchon, Ch.Dieppedale and T.Ouisse, "Modeling of dielectric charging in electrostatic MEMS switches," *Microelectronics Reliability*, vol. 50, pp. 1609-1614, 2010.

[8] S.T.Patton et J.S.Zabinski, «Effects of dielectric charging on fundamental forces and reliability in capacitive microelectromechanical systems radio frequency switch contacts,» *Journal of Applied Physics*, vol. 99, p. 094910, 2006.

[9] M.Lamhamdi, J.Gustavino, L.Boudou, Y.Segui, P.Pons, L.Bouscayrol and R.Plana, "Charging-Effects in RF Capacitive Switches Influence of insulating layers composition," *Microelectronics Reliability*, vol. 46, pp. 1700-1704, 2006.

[10] N. Tavassolian, «Optimization of dielectric material stoichiometry for high reliability capacitive MEMS switches,» *IEEE Microwave and wireless components letters*, p. 1531, 2016.

[11] M. Atienza, S. Gorreta, J. Pons-Nin and M. Dominguez-Pumar, "Characterization of dielectric charging in MEMS using diffusive representation," *IEEE Transactions on Industrial Electronics*, vol. 64, p. 1529, 2017.

[12] P. Giounanlis, D. Andrade-Miceli, S. Gorreta, J. Pons-Nin, M. Dominguez-Pumar and E. Blokhina, "Circuit modeling of a MEMS Varactor Including Dielectric Charging Dynamics," *27th Micromechanics and Microsystems Europe Workshop*, vol. 757, 2016.

[13] A.Jain, S.Palit and M.A.Alam, "A physics-based predictive modeling framework for dielectric charging and creep in RF MEMS capacitive switches varactors," *Journal of microelectromechanical systems*, vol. 21, pp. 420-430, 2012.

[14] M. Koutsoureli, L. Michalas, E. Papandreou and G. Papaioannou, "Induced charging phenomena on SiNx dielectric films used in RF MEMS capacitive switches," *Microelectronics reliability*, vol. 55, pp. 1911-1915, 2015.

[15] S. Ogden, T.-M. Lu and J. Plawsky, "Electron transport and dielectric breakdown in silicon nitride using a charge transport model," *APL*, vol. 109, p. 152904, 2016.

[16] W.M.VanSpengen, «Capacitive RF MEMS switch dielectric charging and reliability: a critical review with recommendations,» *Journal of Micromechanics and Microengineering*, vol. 22, pp. 1-23, 2012.

[17] A.Soma and G.DePasquale, "MEMS Mechanical Fatigue: Experimental Results on Gold Microbeams," *Journal of Microelectromechanical Systems*, vol. 18, pp. 828-835, 2009.

[18] S.Mellé, D.De Conto, L.Mazenq, D.Dubuc, B.Poussard, C.Bordas, K.Grenier, L.Bary, O.Vendier, J.L.Muraro, J.L.Cazaux and R.Plana, "Failure Predictive Model of Capacitive RF-MEMS," *Microelectronics Reliability*, vol. 45, pp. 1770-1775, 2005.

[19] R.W.Herfst, H.G.A.Huizing, P.G.Steeneken and J.Schmitz, "Characterization of dielectric charging in RF MEMS capacitive switches," *IEEE*, pp. 133-136, 2006.

[20] Z.Peng, X.Yuan, J.C.M.Hwang, D.I.Forehand et C.L.Goldsmith, «Superposition Model for Dielectric Charging of RF MEMS Capacitive Switches Under Bipolar Control-Voltage Waveforms,» *IEEE Transactions on Microwave Theory and Techniques*, vol. 55, pp. 2911-2918, 2007.

[21] R.Ramprasad, "Phenomenological theory to model leakage currents in metal-insulator-metal capacitor systems," *Physica Status Solidi (B)*, vol. 239, pp. 59-70, 2003.

[22] G.Papaioannou, F.Coccetti and R.Plana, "On the modeling of dielectric charging in RF-MEMS capacitive switches," *IEEE Topical Meeting on Silicon Monolithic Integrated Circuits in RF Systems (SiRF)*, pp. 108-111,

2010.

[23] A. Amiaud, A. Leuliet, B. Loiseaux, J.-P. Ganne et J. Nagle, «Modeling of dielectric charging in capacitive structures,» *Journal of Applied Physocs*, vol. 118, p. 174103, 2015.

[24] M.Bose, D.K.Basa and D.N.Bose, "Electrical conduction studies of plasma enhanced chemical vapor deposited silicon nitride films," *Journal of Vacuum Science & Technology A : Vacuum, Surfaces, and Films*, vol. 19, Jan/Feb 2001.

[25] X.Yuan, Z.Peng, J.C.M.Hwang, D.Forehand et C.L.Goldsmith, «Acceleration of Dielectric Charging in RF MEMS Capacitive Switches,» *IEEE Transactions on Device and Materials Reliability*, vol. 6, pp. 556-563, 2006.

[26] Z.Peng, C.Palego, J.C.M.Hwang, D.I.Forehand, C.L.Goldsmith, C.Moody, A.Malczewski, B.W.Pillans, R.Daigler et J.Papapolymerou, «Impact of Humidity on Dielectric Charging in RF MEMS Capacitive Switches,» *IEEE Microwave and Wireless Components Letters*, vol. 19, pp. 299-301, 2009.